Development 136, 2069-2079 (2009) doi:10.1242/dev.026435

The novel protein kinase Vlk is essential for stromal function of mesenchymal cells

Masaki Kinoshita*, Takumi Era, Lars Martin Jakt and Shin-Ichi Nishikawa

From a list of protein kinases (PKs) that are newly induced upon differentiation of mouse embryonic stem cells to mesendoderm, we identified a previously uncharacterized kinase, *Vlk* (vertebrate lonesome kinase), that is well conserved in vertebrates but has no homologs outside of the vertebrate lineage. Its kinase domain cannot be classified into any of the previously defined kinase groups or families. Although *Vlk* is first expressed in E-cadherin-positive anterior visceral endoderm and mesendoderm, its expression is later confined to E-cadherin-negative mesenchyme. *Vlk* is enriched in the Golgi apparatus and blocks VSVG transport from the Golgi to the plasma membrane. Targeted disruption of *Vlk* leads to a defect in lung development and to delayed ossification of endochondral bone. *Vlk*$^{-/-}$ mice display neonatal lethality due to respiratory failure, with a suckling defect arising from a cleft palate. Our results demonstrate that Vlk is a novel vertebrate-specific PK that is involved in the regulation of the rate of protein export from the Golgi, thereby playing an important role in the formation of functional stroma by mesenchymal cells.

KEY WORDS: ES cell, In vitro differentiation, Protein kinase, Mesendoderm, AW548124 (Pkdcc), Vlk, Cleft palate, Lung hypoplasia, Delayed chondrocyte hypertrophy

INTRODUCTION

Gene mining has been facilitated by the recent completion of the whole-genome sequences of an increasing number of species, and by the development of high-throughput technologies, such as DNA microarrays, to detect gene expression. Among various settings for gene mining, in vitro differentiation of embryonic stem (ES) cells towards specific lineages has emerged as a promising experimental system that has marked advantages over study of the embryo itself, from which only small numbers of cells can be obtained (Hirashima et al., 2004; Keller et al., 1993; Nishikawa et al., 1998). We have been using ES cell differentiation in combination with high-throughput technologies to identify genes that are involved during early embryogenesis (Takebe et al., 2006).

Protein kinases (PKs), which constitute one of the largest eukaryotic gene families, regulate a variety of cellular processes. Mutation and dysregulation of a variety of PK genes have been implicated as causes of disease, including cancer. The way in which PKs have been studied has changed markedly with the completion of numerous whole-genome sequencing projects. A list of genes encoding PKs, including more than 500 PKs in both human (Manning et al., 2002) and mouse (Caenepeel et al., 2004) genomes, is now available (http://kinase.com). However, a proportion of these PKs remain functionally uncharacterized. Human PKs have been classified into a hierarchy of groups, families and subfamilies according to the sequence of the catalytic domain (Hanks and Hunter, 1995; Hanks et al., 1988). As each family contains well-characterized PKs, this hierarchy is being used to gain insight into the potential functions of PKs. Phylogenetic comparison is another means of investigating the functional significance of PKs. Indeed, most human PKs (510 of 518) have mouse orthologs, and the functions of many PKs are preserved across species. However, this 'kinome' map also contains a few genes that cannot be fully classified into any of the characterized families. Thus, it is still important to assess their expression pattern and function on an individual basis.

In this study, we attempted to list PKs that are newly induced after differentiation to mesendoderm in ES cell culture. Among PKs that are found in mesendoderm cells but not ES cells, we found one PK, Vlk, that could not be classified into any known PK family. This previously uncharacterized PK is unusual in that it has no homologs in invertebrates, although it is highly conserved in vertebrates. We show here that expression of Vlk retards protein transport from the Golgi. Analysis of *Vlk*$^{-/-}$ mutant mice showed that a functional environment for the organogenesis of lung, bone and palate is disturbed.

MATERIALS AND METHODS

Histological analysis, immunofluorescence and the VSVG-GFP transport assay

GFP and Venus proteins were detected using rabbit anti-GFP antibody (Molecular Probes). Goat anti-SP-C, anti-aquaporin 5 and anti-CC10 antibodies (Santa Cruz) were used in lung sections. Rat anti-BrdU antibody (Serotec) was used in the proliferation studies (2-hour labeling of pregnant mother). Paraffin sections and cryosections were 6 μm and 8 μm, respectively. NIH3T3 cells stably expressing *Vlk-GFP* or transiently expressing *VSVG-GFP* (constructs kindly provided by Dr Jennifer Lippincot-Schwartz, NIH) were stained with mouse anti-p115, anti-GM130, anti-Vti1a, anti-GS15 (BD Pharmingen), rabbit anti-TGN38 (Abcam) or rabbit anti-calreticulin (StressGen) antibodies. Fluorescent secondary antibodies from Molecular Probes and HRP-conjugated antibodies from Jackson ImmunoResearch were used.

In the VSVG-GFP transport assay, cells were cultured at 40°C overnight after transfection and 100 μg/ml cycloheximide was added 30 minutes before the temperature shift to 32°C. For FACS analysis of VSVG-GFP, anti-VSVG (8G5) (kindly provided by Dr Douglas S. Lyles, Wake Forest University) and anti-mouse-Alexa633 (Molecular Probes) antibodies were used.

Cell culture and in vitro ES cell differentiation

EB5 and Gsc$^{Gfp+/-}$ EB5 cell lines were maintained as described previously (Tada et al., 2005; Yasunaga et al., 2005). Mesendoderm induction was performed as described previously (Tada et al., 2005). For gene targeting,

Laboratory for Stem Cell Biology, RIKEN Center for Developmental Biology, 2-2-3 Minatojima-Minamimachi, Chuo-ku, Kobe 650-0047, Japan.

*Author for correspondence (e-mail: mask@cdb.riken.jp)

Accepted 20 April 2009

the TT2 ES cell line was maintained as described previously (Yagi et al., 1993). HEK293T cells, NIH3T3 cells, and their derivatives were maintained in DMEM containing 10% FCS.

Microarrays, data analysis and cDNA cloning

Differentiated cells were purified by FACS at each time point. RNA extraction using Trizol (Invitrogen), cRNA probe preparation and hybridization to Affymetrix oligonucleotide arrays MGU74v2 A, B and C were performed as recommended by the manufacturers, as described previously (Takebe et al., 2006). The expression data were maintained and analyzed using the eXintegrator system (http://www.cdb.riken.jp/scb/documentation/). Probe sets representing kinase genes were identified by searching for the term 'kinase' in the Ensembl (version 42) annotation for genes associated (by eXintegrator) with probe sets. These probe sets were then sorted by their similarity (Euclidean distance) to a specified profile with low or non-existent signals in ES and day-5 Gsc^+ E-cadherin$^-$ samples and high signals in day-4 and day-5 Gsc^+ E-cadherin$^+$ samples. The comparison was carried out using an eXintegrator function that compares the individual probe-pair profiles against the specified profile and uses the mean Euclidean distance. The expression data for the resulting list of genes were then manually inspected to remove genes with expression in the ES samples and probe sets with ambiguous identities (i.e. mapping to intronic sequences). The top 36 probe sets were selected for further consideration and are listed in Table 1. Additional annotation, as well as confirmation of the probe set to gene relationships, were obtained from the Ensembl mart_42 database (ArrayExpress accession number E-MEXP-1672).

A cDNA clone representing the *Vlk* transcript was isolated from a lambda phage cDNA library constructed from mRNA of day-4 differentiated CCE ES cells (Nishikawa et al., 1998). The phylogenetic relationship of the *Vlk* sequence was determined by ClustalX (Thompson et al., 1997) followed by MEGA4 (Tamura et al., 2007). Kinase subdomains in Vlk were identified by first aligning the Vlk peptide sequence to the Pfam13.0 kinase hidden Markov model (PF000069.11) using the HMMER package (http://hmmer.janelia.org/). This alignment was then visually inspected for the conserved domains reported previously (Hanks and Hunter, 1995; Hanks et al., 1988).

Generation of knock-in mice

The targeting vector was constructed according to the method described previously (Ikeya et al., 2005). The genomic DNA of G418-resistant colonies was digested with *Sac*I and analyzed by Southern blotting. The PGK-Neo cassette was removed by transient expression of Cre or crossing of chimeric mice with EIIa-Cre mice (Jackson Laboratory). Correctly targeted clones were injected into ICR embryos. The RIKEN accession number of Vlk knock-in mice is CDB0434K.

Whole-mount and section in situ hybridization

In situ hybridization was performed as described previously (Takebe et al., 2006). The mouse *Vlk* probe was amplified by RT-PCR using primers 5′-TGGAGACAGCGCTACACTTG-3′ and 5′-CCCAGTTAAGACCA-GCCTGA-3′. For chick *Vlk*, 5′-GCTACACCAAGGCCGTCTAC-3′ and CCTGTCCAAGTCGTCTGGTT-3′ were used; for zebrafish *Vlk*, 5′-GTGGACGGAGTGTTGAAGGT-3′ and 5′-GCACCGGTCTTAAAG-AGCAC-3′ were used. Type II collagen alpha I (*Col2a1*) and type X collagen alpha I (*Col10a1*) constructs were kindly provided by Dr B. R. Olsen (Harvard Medical School).

Transfection, immunoprecipitation, western blotting and mass spectrometry analysis

Transient transfection was performed using TransIt LT-1 (Mirus Bio). Cells were lysed with buffer [20 mM HEPES pH 7.5, 3 mM $MgCl_2$, 100 mM NaCl, 1 mM DTT, 100 mM Na_3VO_4, 10 mM NaF, 20 mM beta-glycerophosphate, protease inhibitor cocktail (Nacalai), 1 mM EDTA, 1% Triton X-100]. Immunoprecipitation was performed using protein G-agarose (Roche). Anti-phosphotyrosine (Upstate), anti-V5 (Invitrogen), anti-GFP (Molecular Probes) and anti-Vlk (clone 7F2, raised in our laboratory) were used. After SDS-PAGE, staining was performed with ProQ Diamond (Invitrogen) or CBB Stain One (Nacalai). For mass spectrometry analysis, protein bands were excised from CBB-stained gels, trypsinized and analyzed by LC/MS-MS.

Skeletal preparation

Alizarin Red and Alcian Blue staining of P0 skeletons was performed as described previously (Kimmel and Trammell, 1981).

RESULTS

Identification of kinase genes in early ES cell culture

We previously reported a defined culture condition that allows the selective differentiation of mouse ES cells into $goosecoid^+$ (Gsc^+) mesendodermal cells, which subsequently differentiate into E-$cadherin^+$ (E-cad; Cdh1 – Mouse Genome Informatics) definitive endoderm and E-cad^- mesoderm (Tada et al., 2005). During this process, the growth requirements of the differentiating cells change markedly from those of ES cells. In this study, we compared ES and differentiated mesendoderm cells in terms of expression of PKs. We first listed PKs that are expressed in mesendoderm but are not detectable in ES cells (Table 1). A number of these PKs have been implicated in stress responses [*Erk5* (*Mapk7*), *Mapkapk3*, *Map3k7*, *Map2k4*, *Jnk* (*Mapk8*), *Map2k5* and *Ikkb* (*Ikbkb*)], suggesting that some of the genes are induced as a stress response to the defined culture condition.

We were also intrigued by the existence of a PK represented by the Affymetrix 104066_at probe set and identified by MGI symbol *AW548124* (*Pkdcc*), but about which nothing has been reported. One reason for this gene remaining unnoticed in the mouse might be that the genomic sequence upstream of this gene was not clearly defined, resulting in a predicted protein of 293 amino acids containing only a partial kinase domain. However, we isolated a cDNA clone containing the missing upstream sequence and demonstrated the presence of further coding sequence. We found that this gene encodes an mRNA of 2440 nt (DDBJ accession number AB381893) and a protein of 492 amino acids that contains a putative kinase domain.

Interestingly, we failed to find any homologous proteins in invertebrates by BLAST search using a stretch of sequence encoding 237 amino acids (138-374) in the kinase domain, whereas an ortholog of this protein exists in every vertebrate species for which the whole-genome sequence is available. Protein alignment reveals a high degree of conservation between the mouse, human, rat and zebrafish proteins (see Fig. S1A in the supplementary material). The human ortholog, designated *SGK493*, comprises a solitary branch without any other members that stems directly from the origin according to the map of the human kinome (http://kinase.com). In this tree, seven more such solitary branches, each of which has only one member, are present. We performed a TBLASTN search using a 237 amino acid stretch of the kinase domain over the nucleotide collection database (nr/nt). The results of the TBLASTN search were aligned using ClustalX (Thompson et al., 1997) and clustered using MEGA4 (Tamura et al., 2007). The phylogenetic tree of the TBLASTN results and of vertebrate Vlk proteins are shown in Fig. S1B,C in the supplementary material. The BLAST results revealed no invertebrate homologs, despite the high degree of conservation among vertebrates. Although there were a number of hits in plant and invertebrate genes, the homology was not significant. Because of this feature, we named this gene vertebrate lonesome kinase (*Vlk*).

Vlk expression pattern in pre- to mid-gastrulation mouse embryos

During mesendoderm differentiation of ES cells, *Vlk* begins to be expressed in mesendodermal cells on differentiation day 4, as assessed by RT-PCR, and is then expressed only in E-cad^+ endoderm precursor cells but not in E-cad^- cells (data not shown). We

Table 1. List of PKs upregulated during mesendoderm differentiation

Rank	Value*	Affimetrix ID	Group	Family	Gene (source)
1	0.140874	104066_at	Other	Other – unique	Expressed sequence AW548124 (MGI:2147077)
2	0.184352	98452_at	TK	VEGFR	FMS-like tyrosine kinase 1 (MGI:95558)
3	0.189161	163489_at	TKL	RIPK	receptor-interacting serine-threonine kinase 4 (MGI:1919638)
4	0.191523	111233_at	AGC	PKC	protein kinase C, eta (MGI:97600)
5	0.196463	113139_at	CAMK	TRBL	tribbles homolog 2 (Drosophila) (MGI:2145021)
6	0.227337	112692_at	STE	STE20	RIKEN cDNA 2610018G03 gene (MGI:1917665)
7	0.244947	114748_at	CAMK	DAPK	death associated protein kinase 1 (MGI:1916885)
8	0.311274	114925_at	STE	STE20	TRAF2 and NCK interacting kinase (MGI:1916264)
9	0.325234	115909_at	CAMK	CAMKL	SNF1-like kinase 2 (MGI:2445031)
10	0.328924	112442_at	TK	ACK	tyrosine kinase, non-receptor, 1 (MGI:1930958)
11	0.342771	106573_at	CAMK	CAMKL	SNF related kinase (MGI:108104)
12	0.353542	117151_at	TK	MET	met proto-oncogene (MGI:96969)
13	0.356705	112983_at	TK	ROR	receptor tyrosine kinase-like orphan receptor 1 (MGI:1347520)
14	0.36157	107580_g_at	AGC	DMPK	Cdc42 binding protein kinase beta (MGI:2136459)
15	0.393467	163536_at	CK1	CK1	casein kinase 1, gamma 3 (MGI:1917675)
16	0.395264	107465_at	CAMK	CAMK1	calcium/calmodulin-dependent protein kinase ID (MGI:2442190)
17	0.413686	110852_at	Atypical	PIKK	transformation/transcription domain-associated protein (MGI:2153272)
18	0.414039	92427_at	TKL	STKR	transforming growth factor, beta receptor I (MGI:98728)
19	0.425736	115874_at	STE	STE20	p21 (CDKN1A)-activated kinase 1 (MGI:1339975)
20	0.429529	141026_at	Other	NKF3	Adult male bone cDNA, RIKEN full-length enriched library, clone: 9830148H23 product: hypothetical protein kinase-like (PK-like) structure containing protein, full insert sequence (DNA segment, Chr 8, ERATO Doi 82, expressed) (Uniprot/SPTREMBL;Acc:Q8CB68)
21	0.433359	103592_at	STE	STE7	mitogen activated protein kinase kinase 5 (MGI:1346345)
22	0.436237	117265_at	Other	SCY1	SCY1-like 1 (S. cerevisiae) (MGI:1931787)
23	0.438849	105742_at	AGC	AKT	thymoma viral proto-oncogene 3 (MGI:1345147)
24	0.44402	132114_f_at	Other	WNK	WNK lysine deficient protein kinase 4 (MGI:1917097)
25	0.449448	167725_f_at	CMGC	CDK	PFTAIRE protein kinase 1 (MGI:894318)
26	0.454032	168469_f_at	Other	NKF2	PTEN induced putative kinase 1 (MGI:1916193)
27	0.456906	111539_at	Other	SCY1	SCY1-like 2 (S. cerevisiae) (MGI:1289172)
28	0.458283	105428_at	CAMK	MAPKAPK	mitogen-activated protein kinase-activated protein kinase 3 (MGI:2143163)
29	0.464858	108785_at	STE	STE11	mitogen activated protein kinase kinase kinase 7 (MGI:1346877)
30	0.468153	93723_at	TK	ROR	receptor tyrosine kinase-like orphan receptor 2 (MGI:1347521)
31	0.47274	99388_at	TK	SRC	Rous sarcoma oncogene (MGI:98397)
32	0.475296	112462_at	CMGC	DYRK	homeodomain interacting protein kinase 3 (MGI:1314882)
33	0.49409	99000_at	CMGC	MAPK	mitogen activated protein kinase 7 (MGI:1346347)
34	0.51967	111507_at	STE	STE7	mitogen activated protein kinase kinase 4 (MGI:1346869)
35	0.521478	138075_at	CMGC	MAPK	mitogen activated protein kinase 9 (MGI:1346862)
36	0.572143	162716_at	Other	IKK	inhibitor of kappaB kinase beta (MGI:1338071)

PKs expressed in ES cell-derived mesendoderm cells are listed (PKs that are expressed in ES cells are excluded from this list).
*Value indicates a distance measurement based on Euclidean distances to a specified profile.

examined the correlation of this gene expression pattern with that in embryos by whole-mount in situ hybridization. Whereas *Vlk* expression was detected in the anterior endoderm in late gastrulation embryos (Fig. 1B), we failed to detect a signal in the organizer region of gastrulating embryos (E6.5-7.5) corresponding to the earliest mesendoderm detected in culture. As it is possible that this failure was due to insufficient detection sensitivity, we attempted to increase the sensitivity using a reporter gene, the expression of which corresponds to that of the endogenous *Vlk* gene. For this purpose, we established a mouse strain in which the *Venus* reporter gene (Nagai et al., 2002) was inserted into the *Vlk* allele (see Fig. S3 in the supplementary material). Consistent with our expectations, the reporter gene expression pattern indicated that *Vlk* begins to be expressed in the organizer region at the onset of gastrulation (~E6.5) as well as in the anterior visceral endoderm (AVE) (Fig. 1A). At the late gastrula stage, *Vlk* was detectable in the node region in addition to the AVE (Fig. 1B-D). During gastrulation, the highest level of *Vlk* expression was found in the AVE. These results indicate that the in vitro expression pattern of *Vlk* is largely consistent with that observed in the embryo.

We also analyzed the expression of *Vlk* orthologs in gastrulae of zebrafish and chicken by in situ hybridization (see Fig. S2 in the supplementary material). In zebrafish, expression was first detected in the shield corresponding to the organizer at 6 hours post-fertilization (hpf) (see Fig. S2A in the supplementary material). At 12 hpf, expression was confined to head ectoderm and mesoderm (see Fig. S2B in the supplementary material). In the chick gastrula, *Vlk* expression was detectable only in the anterior endoderm (see Fig. S2C in the supplementary material). Although we failed to detect expression in the chick organizer, the overall expression pattern of *Vlk* appears to be largely preserved in vertebrate gastrula.

Vlk expression in the E8-10 mouse embryo

Using the *Venus* reporter mouse strain described above, *Vlk* expression was detected mainly in mesenchymal cells, but not in the E-cad^{+} populations in embryos, including the definitive endoderm and embryonic ectoderm. In E9.5 embryos, the strongest levels of expression were observed in the branchial arches and limb buds (Fig. 1E-G), tissues in which mesenchymal cells are condensed. Double staining of sections for E-cad showed that *Vlk* is not

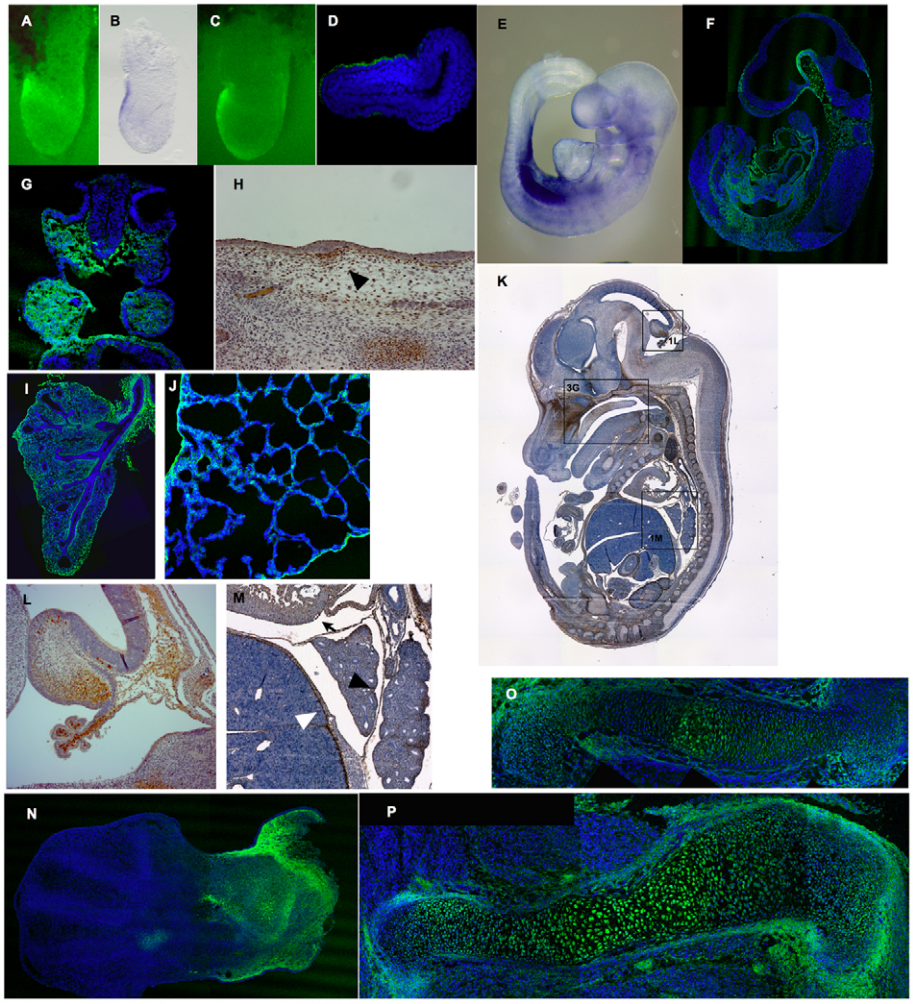

Fig. 1. Expression pattern of *Vlk* during mouse development. Detection of *Vlk* transcript (blue) (B,E) and Venus reporter expression (green in A,C,D,F,G,I,J,O,P; brown in H,K,L,M) in whole-embryo (A-C,E), confocal section (D) and embryo sections (F-P). (**A**) In E6.5 embryos, *Vlk* is expressed in the anterior visceral endoderm (AVE) and gastrula organizer as shown by Venus expression (lateral view). (**B-D**) At E7.5, expression was observed in the AVE and node. (**E-G**) At E9.5, *Vlk* is expressed in the mesenchyme in the limb buds (E), branchial arch (G) and cardiac mesoderm (E,F). (**H**) Expression of *Vlk* was observed in condensed mesenchyme under the skin at E14.5 (arrowhead). (**I**) In E13.5 lung, expression of *Vlk* is present in almost all mesenchymal and mesothelial cells, with the strongest expression seen in the peri-bronchial mesenchyme. (**J**) Broad expression was lost in the P0 lung mesenchyme but continued in the mesothelium. (**K**) Pattern of *Vlk* expression in E14.5 embryo (sagittal section). (**L**) Magnified view from K, showing expression of *Vlk* in the choroidal plexus of E14.5 embryos. (**M**) Magnified view from K, showing expression of *Vlk* in various mesothelia, such as the peritoneum (white arrowhead), pleura (black arrowhead) and pericardium (black arrow). (**N**) In the E12.5 forelimb, *Vlk* is expressed in condensed mesenchyme that is differentiating into chondrocytes. (**O**) In the humerus bone at E13.5, *Vlk* expression was observed in proliferating chondrocytes and reserve chondrocytes. (**P**) At E14.5, strong *Vlk* expression was observed in hypertrophic chondrocytes.

expressed in most of the endodermal cells, except for a small number of double-positive cells in the foregut at E9.5 (data not shown). Although most neuronal cells were negative for *Vlk* expression, expression was detected in neuronal cells in the ventral part of the mid-brain (Fig. 1F).

Vlk expression pattern during organogenesis

During mid-gestation, *Vlk* expression in mesenchymal cells continues (Fig. 1K shows the *Vlk* expression pattern in an E14.5 sagittal section). Its expression was particularly conspicuous in areas where mesenchymal cells condense, such as beneath the hair bud (Fig. 1H), the lining of the developing bronchial tree (Fig. 1I), in cells aligned with the elongating choroidal plexus (Fig. 1L) and in regions of chondrogenesis and osteogenesis (Fig. 1N-P). Similarly, the mesothelium wrapping the visceral organs, such as the peritoneum, pericardium and pleura (Fig. 1M), which are derived from mesenchymal cells, showed high levels of *Vlk* expression, suggesting that *Vlk* is expressed in mesenchymal cells undergoing dynamic change.

Vlk expression in mesenchymal cells was further examined during limb bone formation (especially of the humerus) and lung organogenesis as we found defects in the formation of these tissues in *Vlk*-null mutant mice (as described below). Expression of *Vlk* was detected throughout all stages of humerus bone formation. During limb formation, condensed mesenchymal cells in the limb bud expressed *Vlk*. *Vlk* expression decreased in chondrocytes as they differentiated from condensed mesenchyme, whereas expression remained stable in the perichondrium. No *Vlk* expression was found in digit chondrocytes at E12.5 (the developing paw showed no *Vlk* expression), whereas strong expression was observed in the primordium of the more-proximal bone (Fig. 1N). *Vlk* expression in chondrocytes regained strength as they became hypertrophic, and *Vlk* continued to be expressed during osteogenesis (Fig. 1M,P). Thus, the *Vlk* expression level fluctuates during the development of skeletal bones, and its expression level is high at the transition stages from mesenchymal cells to chondrocytes and from chondrocytes to osteoblasts.

Lung development in mice has been classified into four stages involving tracheal bud generation: the pseudoglandular stage (E9.5-16.5), with generation of tracheal branching; the canalicular (E16.5-17.5) and saccular stages (E17.5-P5), with generation of alveoli; and the alveolar (P5-30) stage involving the maturation of alveolar ducts and alveoli. Expression of *Vlk* was observed in all mesenchymal cells in the lung at the early pseudoglandular stage (E13.5, Fig. 1I). The highest level of expression at this stage was in the condensed mesenchymal cells lining the developing trachea (Fig. 1I). However, expression was rapidly lost from the mesenchyme of the lung interstitium during the mid-to-late pseudoglandular stage. By contrast, at P0 (saccular stage), the mesenchymal cells in the subpleural region and the pleural cells themselves continued to express *Vlk* (Fig. 1J). The mesothelial pleural cells continue to express *Vlk* throughout life (data not shown).

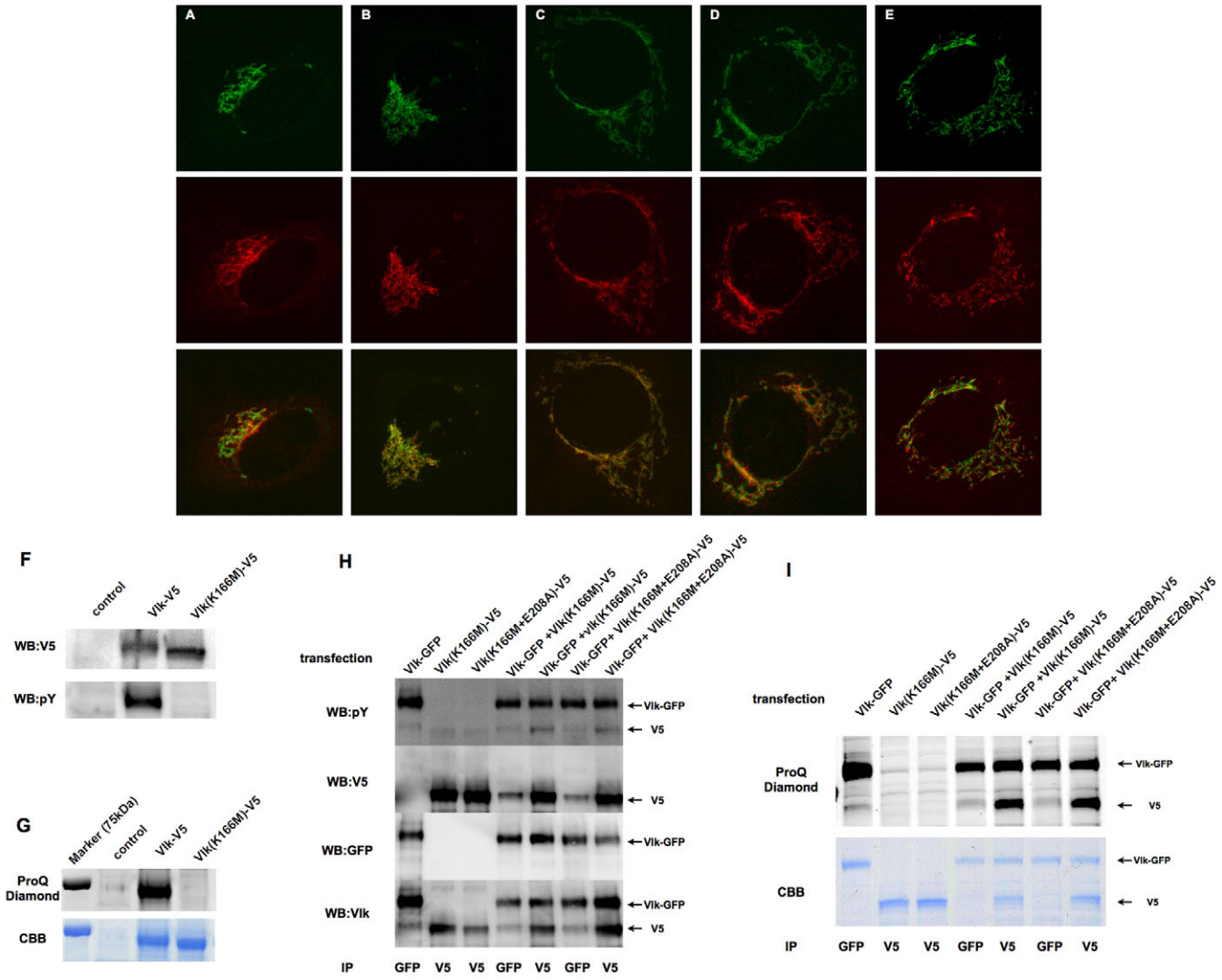

Fig. 2. Subcellular localization and kinase activity of Vlk. (**A-E**) The *Vlk-GFP* fusion gene was introduced into mouse NIH3T3 cells and co-immunostained with antibodies against p115 (A), GM130 (B), GS15 (C), Vti1a (D) and TGN38 (E). Vlk-GFP is shown in green and Golgi markers in red. (**F**) *V5*-tagged *Vlk* was transiently expressed in human HEK293T cells and immunoprecipitated with anti-V5 antibody. WT Vlk was tyrosine phosphorylated, whereas the K166M-Vlk was not. (**G**) Phosphorylation of WT Vlk-V5 was confirmed by staining with ProQ Diamond. (**H**,**I**) Mutant forms of Vlk (K166M or K166+E208A) were phosphorylated when co-transfected with WT Vlk protein. *V5*- or *GFP*-tagged *Vlk* (WT or mutant) were introduced into HEK293T cells, and protein complexes were immunoprecipitated with anti-GFP or anti-V5 antibody. Tyrosine phosphorylation status was analyzed by western blotting (anti-pY) or ProQ Diamond staining. CBB, Coomassie Brilliant Blue staining; IP, immunoprecipitation; WB:V5, WB:pY and WB:Vlk, western blotting using anti-V5, anti-phosphotyrosine and anti-Vlk antibody, respectively.

In summary, *Vlk* is first expressed in the mesendoderm of gastrulation stage embryos, including the early organizer and AVE cells. However, after gastrulation, its expression is found mainly in mesenchymal cells. Although most mesenchymal cells express *Vlk* to some degree, its expression level fluctuates. There is a clear tendency for *Vlk* expression to be high at transition phases of mesenchymal cell differentiation, such as from mesenchymal cells to chondrocytes and from mesenchymal to mesothelial cells.

Cell biological analysis of Vlk

To determine the subcellular localization of Vlk, we constructed a *GFP*-tagged *Vlk* chimeric gene. Fig. 2A-E shows double immunostaining of NIH3T3 cells with anti-GFP and antibodies against Golgi proteins, including p115 (Uso1) [from endoplasmic reticulum (ER) exit site through ER-Golgi intermediate compartment (ERGIC) to cis-Golgi], GM130 (Golga2) (ERGIC and cis-Golgi), GS15 (Bet1l) (medial-Golgi), Vti1a (trans-Golgi) and TGN38 (Tgoln1) (trans-Golgi network). The GFP signal overlapped to various degrees with those of GM130 and GS15, but segregated completely from that of TGN38.

The *Vlk* gene product contains at least kinase subdomains I, II, III, IV, VI, VII and VIII (partial match), but lacks subdomain IX (see Fig. S1A in the supplementary material). However, we failed to detect any kinase activity by standard in vitro kinase assays involving autophosphorylation or phosphorylation of myelin basic protein (Mbp) as a target substrate (data not shown). As its putative substrate is unknown, we next analyzed its kinase activity by comparing wild-type (WT) and mutant proteins in transfected cells.

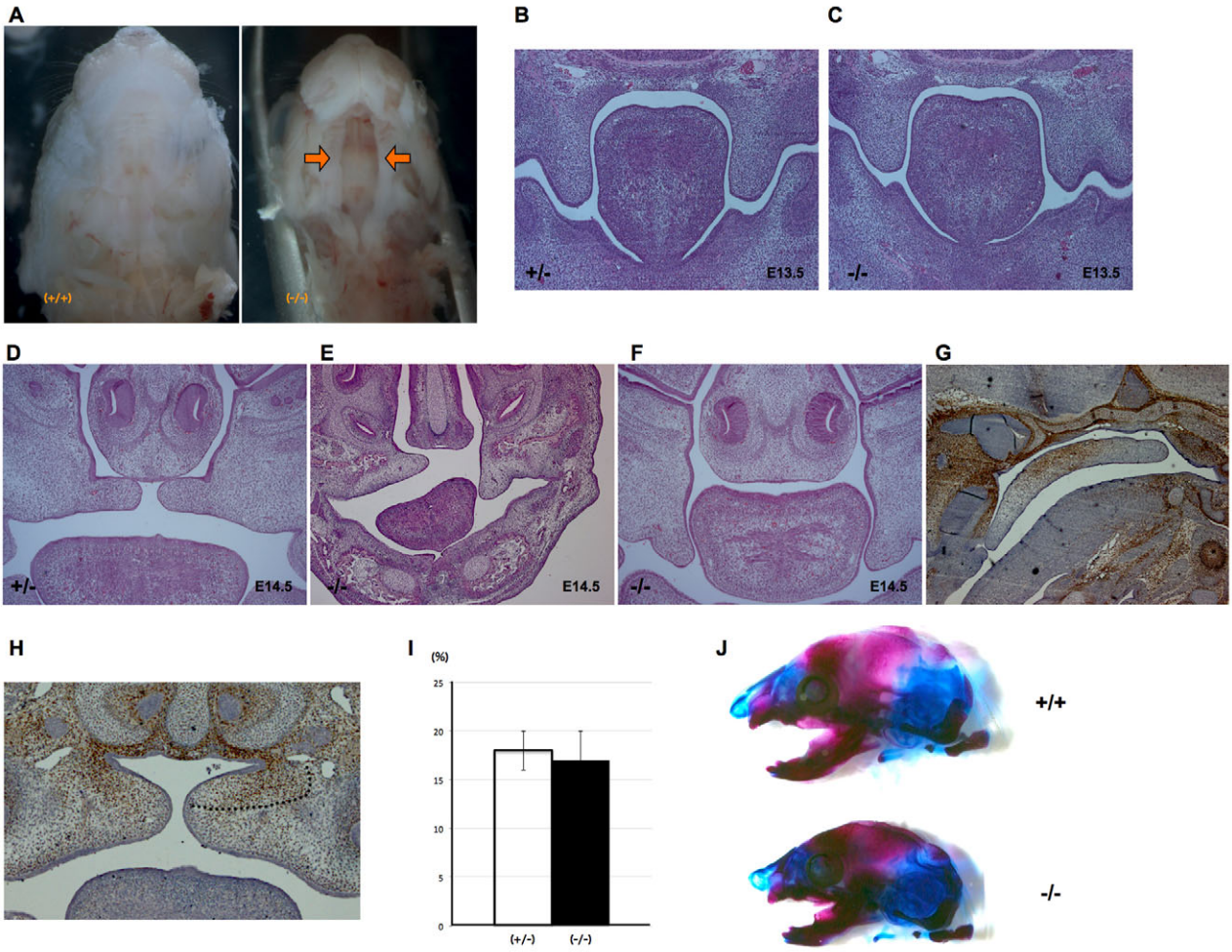

Fig. 3. *Vlk*$^{-/-}$ neonates exhibit a cleft plate. (**A**) *Vlk*$^{-/-}$ mice have a cleft palate (arrows). (**B**,**C**) At E13.5, the palatal shelves are located bilaterally to the tongue in both *Vlk*$^{+/-}$ and *Vlk*$^{-/-}$. (**D-F**) At E14.5, the palatal shelves are elevated and grow in the horizontal direction in *Vlk*$^{+/-}$ embryos. In *Vlk*$^{-/-}$, the palatal shelves fail to elevate, either unilaterally (E) or bilaterally (F). (**G**,**H**) *Vlk* expression in palatal shelves at E14.5. The sagittal section in G shows that *Vlk* is expressed in the middle part (in the anterior-posterior direction) of the developing palatal shelf. In addition, in H, the upper and inner sides of the mesenchyme can be seen to express the *Vlk* gene. (**I**) Percentage of BrdU-positive mesenchymal cells in the region expressing the *Vlk* gene (dotted line in H) was unchanged: 17.9±1.9% in *Vlk*$^{+/-}$ versus 17.3±3.4% in *Vlk*$^{-/-}$. (**J**) Alizarin Red and Alcian Blue staining of the P0 head. The *Vlk*$^{-/-}$ head was smaller and the nasal capsule shorter than in *Vlk*$^{+/+}$ controls.

The *V5*-tagged WT *Vlk* gene introduced into HEK293T cells was tyrosine phosphorylated, as determined by western blotting with an anti-phosphotyrosine antibody (4G10) following immunoprecipitation by an anti-V5 monoclonal (Fig. 2F). By contrast, no tyrosine phosphorylation was detected when we performed the same assay using a *V5*-tagged *Vlk* gene with a mutation in the putative ATP-binding site (K166M) (Fig. 2F). This result was confirmed by SDS-PAGE and by staining of these immunoprecipitates with ProQ Diamond, which stains phosphoproteins (Fig. 2G). Thus, in vivo tyrosine phosphorylation of Vlk is dependent on the intact kinase domain of Vlk itself, although its activity could not be detected by in vitro autophosphorylation assays. Mass spectrometry analysis identified tyrosine 148 and serine 177 as phosphorylation sites dependent on Vlk. Taken together, these observations suggest that phosphorylation of Vlk requires a phosphorylation cascade in which Vlk itself is involved as a kinase. To test this hypothesis, we investigated whether kinase-dead mutants, such as K166M-Vlk and (K166M+E208A)-Vlk, could be phosphorylated in HEK293T cells when co-expressed with WT Vlk. In this experiment, the WT *Vlk* gene was tagged with GFP to allow it to be distinguished from the mutant *Vlk* gene product. In accordance with our expectations, we detected phosphorylation of the mutant Vlk only when co-transfected with WT Vlk (Fig. 2H,I). Taken together, these observations indicate that Vlk probably has kinase activity and that Vlk autophosphorylation is dependent on this activity. The experiments shown in Fig. 2F-I were also confirmed using the NIH3T3 mesenchymal cell line (not shown).

Analysis of *Vlk*$^{-/-}$ mice

To examine *Vlk* gene function in vivo, we deleted the first 213 amino acids of the N-terminus, including amino acids that form part of kinase subdomains I, II and III, and introduced the *Venus* gene with a stop codon in-frame with the first methionine. This construct should thus lead to disruption of endogenous gene expression. *Vlk*$^{+/-}$ mice are healthy and fertile and we obtained *Vlk*$^{-/-}$ mice by intercrossing *Vlk*$^{+/-}$. *Vlk*$^{-/-}$ mice died soon after birth owing to respiratory failure. Contrary to our expectation from *Vlk* expression during gastrulation, *Vlk*

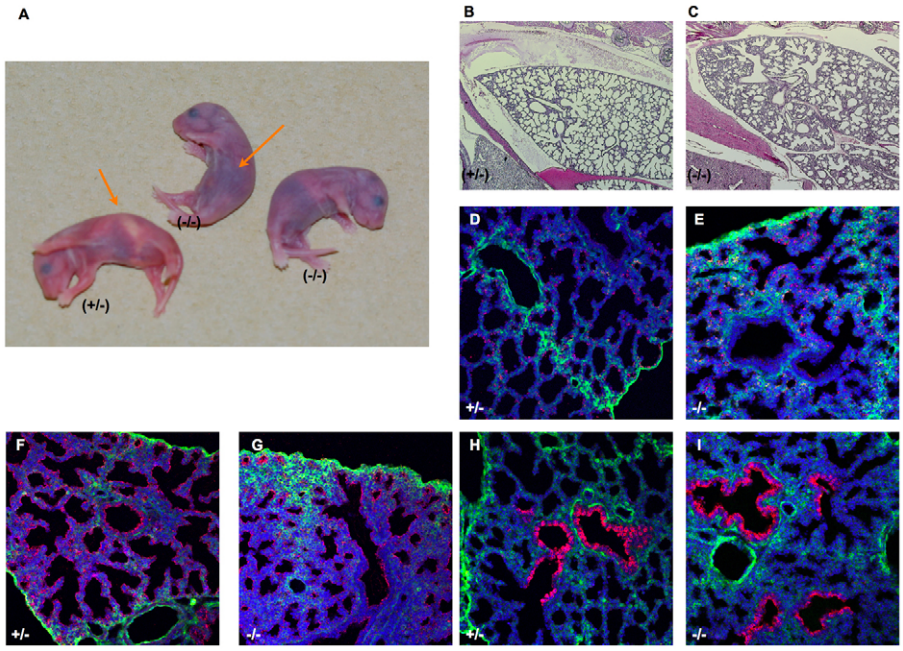

Fig. 4. Lung hypoplasia in *Vlk*$^{-/-}$ mice. (**A**) *Vlk*$^{-/-}$ neonates had cyanosis and suckling defects (arrows). (**B**,**C**) Hematoxylin and Eosin staining of *Vlk*$^{+/-}$ (B) and *Vlk*$^{-/-}$ (C) lung of P0 neonates. In comparison to the *Vlk*$^{+/-}$ lung, the *Vlk*$^{-/-}$ lung had a narrow airspace and thick alveolar septa. (**D-I**) Immunofluorescence images of E18.5 lung sections of *Vlk*$^{+/-}$ and *Vlk*$^{-/-}$. Red signals indicate SP-C (D,E), aquaporin 5 (F,G) or CC10 (H,I). Green signals indicate Venus. Nuclei are blue.

appears to be dispensable for early embryogenesis. *Vlk*$^{-/-}$ neonates showed growth retardation (Fig. 5A), craniofacial abnormalities (Fig. 3I), cleft palate (Fig. 3A), cyanosis and suckling defects (Fig. 4A), shortened limbs and delayed ossification (see Fig. 5B,C).

Cleft palate and cranial abnormalities

At E13.5, the developing palatal shelves are located at the lateral side of the tongue in both *Vlk*$^{+/+}$ and *Vlk*$^{-/-}$ embryos (Fig. 3B,C). At E14.5, the palatal shelves change shape and position, with each palatal shelf elevating above the tongue and growing horizontally in the axial direction before finally fusing at the midline through an epithelial-to-mesenchymal transition (Fig. 3D). In *Vlk*$^{-/-}$ mice, the process of palatal shelf elevation was severely disturbed, either unilaterally (Fig. 3E) or bilaterally (Fig. 3F). This appears to be the cause of the failure of the palate to close in all *Vlk*$^{-/-}$ animals analyzed. Thus, *Vlk* plays an essential role in guiding the direction of palate elongation.

In the developing palatal shelf, stronger expression of *Vlk* was found in the middle part and inner side of the palatal process (Fig. 3G,H). As we could not detect a significant difference between *Vlk*$^{-/-}$ and *Vlk*$^{+/-}$ in the number of proliferating Vlk^{+} mesenchymal cells in the upper half of the palatal shelf (dotted line in Fig. 3H, Fig. 3I) or in the number of cells undergoing apoptosis (data not shown), *Vlk* might be involved in the process of generating some morphogenic constraint that is required to induce the bending of the elongating process inward. Owing to this severe cleft palate, all *Vlk*$^{-/-}$ offspring showed suckling problems as evidenced by the absence of colostrum.

In addition to the cleft palate, *Vlk*$^{-/-}$ mice showed malformation of the craniofacial architecture. Fig. 3J shows Alizarin Red and Alcian Blue staining of head structures in neonates at P0. By comparison with controls, the nasal capsule and maxilla bone were small and severely shortened, although all bones were formed.

Lung hypoplasia

Vlk$^{-/-}$ pups had cyanosis owing to respiratory failure (Fig. 4A). As shown in Fig. 4B,C, the neonatal lung showed enlarged air spaces with a marked decrease in the number of alveoli and an increase in the thickness of the alveolar septum. This phenotype suggests that *Vlk* is involved in alveolus formation by septating alveolar saccules (Massaro and Massaro, 1996). Despite such severe deformity of the lung structure, most offspring survived for a few hours. This is probably because all the components required for formation of the basic architecture necessary for respiratory function were generated in the *Vlk*$^{-/-}$ mice. No significant differences were detected in the expression of surfactant proteins between *Vlk*$^{+/+}$ and *Vlk*$^{-/-}$ mice by RT-PCR (data not shown). Moreover, all types of alveolar and bronchial components were identified by both histological and immunohistological examination of E18.5 lung. The number of type II alveolar cells detected by anti-SP-C (Sftpc) staining was similar in *Vlk*$^{-/-}$ and *Vlk*$^{+/-}$ lung (Fig. 4D,E). Similarly, type I alveolar cells (Fig. 4F,G) and ciliated tracheal cells (Fig. 4H,I) were present in their normal positions. However, in the lungs of *Vlk*$^{-/-}$ mice, SP-C^{+} cells that are normally localized to the epithelial lining of the alveolar lumen were instead found in both the alveolar lining and in the interstitial region (Fig. 4D,E), again suggesting a defect in the sacculation process. However, there were no notable differences in the tissue localization of CC10^{+} (Scgb1a1) tracheal epithelial cells. Taken together, Vlk is involved in the patterning of alveolar cells during the sacculation stage, whereas tracheal development is unaffected in its absence.

It should be emphasized, however, that *Vlk* is expressed in interstitial but not alveolar cells. Moreover, as shown in Fig. 1I, Vlk^{+} mesenchymal cells that are distributed homogeneously over the lung at the pseudoglandular stage move progressively toward the distal region of the lung as the size of the lung increases. Hence, this defect in the formation of alveoli, which occurs during the late pseudoglandular to saccular stage of lung development, should be caused by events during the early pseudoglandular stage when *Vlk* is expressed in the mesenchymal cells adjacent to the developing alveolar cells. Interestingly, the alveolar acinus appears to be assembled within the region where *Vlk* is expressed at high levels. In *Vlk*$^{-/-}$ mice, this acinar formation was significantly retarded, whereas no significant difference was observed in the number of E-cad^{+} cells (data not shown).

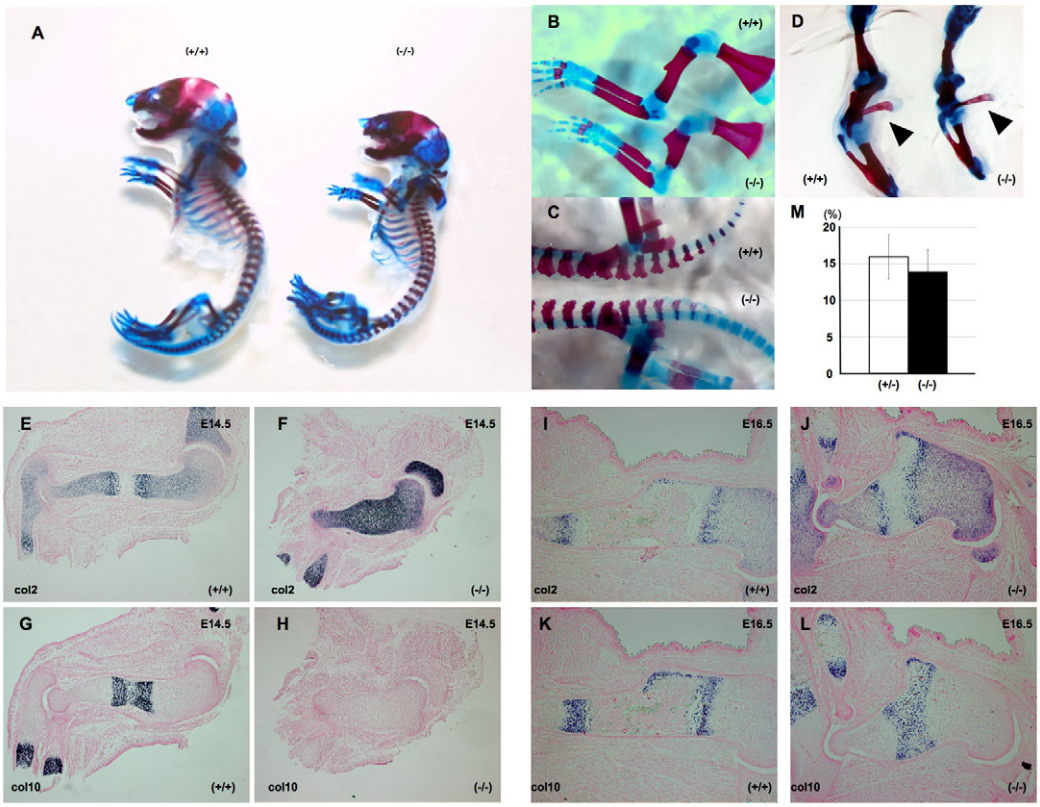

Fig. 5. Chondrocyte hypertrophy is delayed in *Vlk*$^{-/-}$ mice. (**A**) Whole-mount Alizarin Red and Alcian Blue staining of P0 neonates. *Vlk*$^{-/-}$ are smaller than *Vlk*$^{+/+}$ neonates. (**B**) Forelimb of a P0 neonate. Alizarin Red-positive parts of the radius, ulna and humerus are short and thickened in the mutants. (**C**) Ossification in vertebrae was delayed in *Vlk*$^{-/-}$. (**D**) Clavicles (arrowheads) were unaffected in *Vlk*$^{-/-}$. (**E-L**) In situ hybridization of collagen II (E,F,I,J), and collagen X (G,H,K,L) in the developing E14.5 (E-H) and E16.5 (I-L) humerus indicates a delay in the emergence of hypertrophic chondrocytes (collagen X-positive cells) in *Vlk*$^{-/-}$. Sections were counterstained with Nuclear Fast Red. (**M**) The percentage of BrdU-positive cells in proliferating chondrocytes was unchanged: 16.5±3.3% in *Vlk*$^{+/-}$ versus 14.0±2.7% in *Vlk*$^{-/-}$.

Bone formation

All offspring of *Vlk*$^{-/-}$ mice were significantly smaller than those of *Vlk*$^{+/+}$ mice owing to defects in the development of the skeleton. In *Vlk*$^{-/-}$ mice, the ossification of skeletal bone such as limbs and vertebrae, as detected by Alizarin Red staining, was suppressed (Fig. 5A-C). However, there were only minimal differences in membranous bone formation (Fig. 3J; Fig. 5D). As we described previously, a biphasic expression of *Vlk* is observed during limb formation; the first peak occurs during the mesenchymal condensation prior to chondrogenesis, and the second at the stage of hypertrophic chondrocyte differentiation prior to osteogenesis. No defect was detected in the process from mesenchymal condensation to chondrogenesis. However, the differentiation of hypertrophic chondrocytes was markedly retarded. Normally, at E14.5, chondrocytes at the center of the humerus become hypertrophic and lose expression of collagen II mRNA but gain collagen X expression (Fig. 5E,G). In the mutant bone, however, all chondrocytes of E14.5 embryos remained positive for collagen II and no expression of collagen X mRNA was observed (Fig. 5F,H). Differentiation of hypertrophic chondrocytes, as assessed by collagen X expression, was delayed by ~2 days in the *Vlk*$^{-/-}$ embryos (Fig. 5I-L). This delay might result in a subsequent delay of the ossification process, leading to a small body size. As was the case for mesenchymal cells in other regions, we did not find any significant change in BrdU incorporation (Fig. 5M) or any enhancement of apoptosis (data not shown) in proliferating chondrocytes. However, the orientation of chondrocyte growth appeared to be misdirected in the mutant because the humerus became thicker at the expense of length. Taken together, these observations indicate that *Vlk* is involved in the differentiation of hypertrophic chondrocytes rather than in the proliferation or survival of chondrocytes in general.

Retardation of protein transport from the Golgi by *Vlk* expression

The above results strongly suggest that the morphogenetic defects of *Vlk*$^{-/-}$ mutants are due to a failure to form a proper environment for organogenesis, rather than to a cell-autonomous failure. As Vlk is localized at the Golgi apparatus in *Vlk*-transduced cells (Fig. 2A-E) and is involved in stromal function of mesenchymal cells, it is plausible that Vlk is involved in the protein secretion pathway. To test this possibility, we measured vesicular transport using temperature-sensitive vesicular stomatitis virus G (VSVG) protein (ts045) fused to GFP (Hirschberg et al., 1998). In this experimental system, VSVG-GFP is first accumulated in the ER when cultured at 40°C and molecules are released from ER to plasma membrane (PM) through the Golgi apparatus once the temperature is shifted to 32°C. As NIH3T3 is a mesenchymal cell line that does not express *Vlk*, we chose it for assessing the effect of Vlk on vesicular transport. We introduced VSVG-GFP together with WT Vlk, kinase-dead K166M-Vlk, and ΔN-Vlk (which lacks a 30 amino acid sequence at the N-terminus, leading to Vlk mislocalization in the cytoplasm and a lack of phosphorylation; data not shown) constructs into NIH3T3

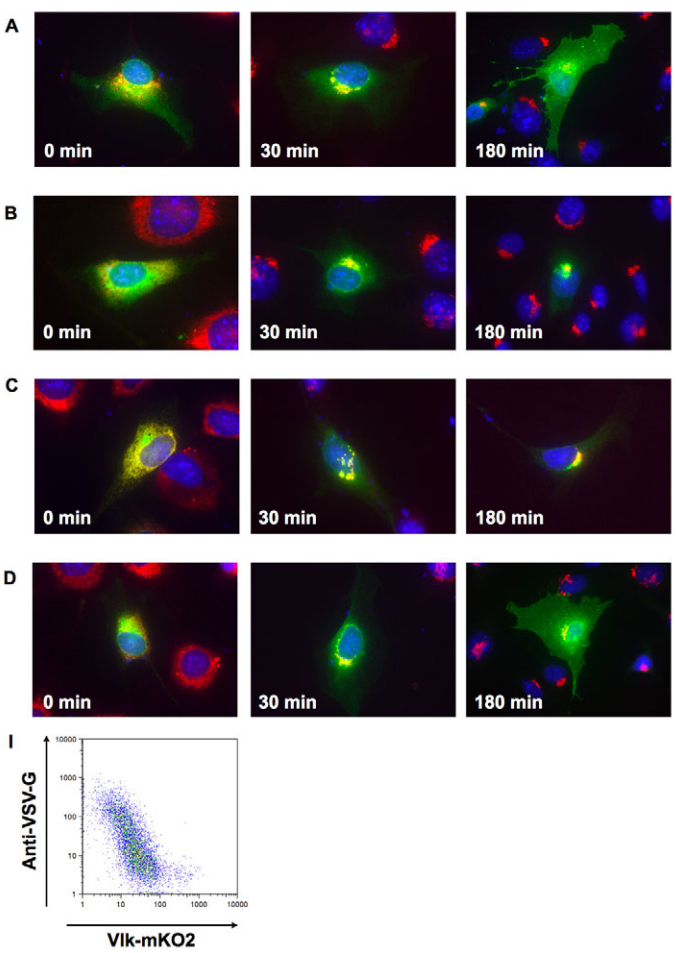

Fig. 6. Inhibition of vesicular transport from the Golgi by Vlk. VSVG-GFP was co-transfected with control (A,E), WT VlK (B,F), K166M-Vlk (C,G) or ΔN-Vlk (D,H) constructs into NIH3T3 cells. (**A-D**) Cells were cultured at 40°C overnight then moved to 32°C; cells were then fixed and stained at each time point. The red signal at 0 minutes is anti-calreticulin staining (endoplasmic reticulum), whereas that at 30 and 180 minutes is anti-GM130 staining (Golgi apparatus). VSVG-GFP signals are green, and nuclei are counterstained with DAPI (blue). (**E-H**) At 180 minutes, cells were analyzed by FACS. A VSVG antibody that recognizes the extracellular domain of the VSVG protein was used. Numbers indicate the proportion of GFP-positive gated cells of each fraction. (**I**) Extracellular VSVG-GFP versus Vlk-mKO (monomeric Kusabira-Orange) analyzed in the GFP-positive gated fraction. The amount of VSVG transported to the plasma menbrane was inversely correlated with the amount of Vlk-mKO.

cells. When co-transfected with the control or ΔN-Vlk construct, VSVG-GFP that localized at the ER at 0 minutes moved to the Golgi apparatus 30 minutes after shifting the temperature to 32°C (Fig. 6A,D). Within 3 hours after the temperature shift, VSVG-GFP was detectable on the PM (Fig. 6A,D). In the cells in which VSVG-GFP was co-transduced with WT or K166M-Vlk, translocation of VSVG-GFP from ER to Golgi occurred normally, but its transport from Golgi to PM appeared to be retarded, as VSVG-GFP accumulated in the Golgi apparatus (Fig. 6B,C). This block from the Golgi to the PM was confirmed by flow cytometry of surface-stained cells 3 hours after the temperature shift. In control- and ΔN-Vlk-transfected cells, the GFP and extracellular VSVG signals lie on a diagonal line (Fig. 6E,H). However, the amount of surface protein relative to the total GFP signal was reduced significantly in WT and K166M-Vlk co-transfected cells (Fig. 6F,G). To clarify the causal role of Vlk in protein transport, we introduced VSVG-GFP and Vlk-mKO [monomeric Kusabira-Orange (Karasawa et al., 2004)] constructs to enable monitoring of both proteins simultaneously. Fig. 6I clearly shows that the amount of VSVG transported to the PM was inversely correlated with the amount of Vlk-mKO. This result indicates that Vlk inhibits protein transport in a dose-dependent fashion.

DISCUSSION

In this study, we first produced a list of PKs that are not expressed in ES cells but are newly induced in the differentiated Gsc^{+} mesendoderm. As many PKs occupy important positions in signal transduction pathways and a classification of all PKs has been completed in both human (Manning et al., 2002) and mouse (Caenepeel et al., 2004), we expected that this line of analysis might provide useful information on the specific signaling network that functions in early intermediate stages such as in the mesendoderm. Contrary to our expectations, excluding all PKs that are detectable in ES cells but that undergo quantitative changes during differentiation turned out not to be useful in revealing novel signals regulating mesendoderm differentiation. With respect to receptor-type PKs, we could identify only Flt1, Met, Ror1 and Ror2 that were known to be dispensable for mesendoderm differentiation. Of interest is that a group of proteins in the MAP kinase signaling pathways are newly expressed upon ES cell differentiation. Some of them, such as Map3k7, Map2k4 and Jnk2 (Mapk9), are implicated in the TGFβ and interleukin signaling pathways (Ninomiya-Tsuji et al., 1999; Su et al., 2006) and might play a role in extrinsic signaling. Alternatively, their expression is a reflection of environmental stress in the defined culture condition, as these proteins are involved in cellular stress responses.

Nearly all PKs in this list have been characterized to some extent and can be classified into one of the known PK families, but we also found one PK that was completely uncharacterized in mice. Judging from the sequence, this mouse PK is an ortholog of human *SGK493*. According to a previous classification of all PKs (Manning et al., 2002) and the results of our own analyses, this PK showed two intriguing features. First, no homolog was detected in invertebrates by BLAST search, whereas orthologs were found in all vertebrates examined. Second, this protein could not be classified into any of the known PK families and constitutes a solitary branch in the

kinome with this PK as a sole member. Because of these two features, we designated this PK vertebrate lonesome kinase (Vlk). The human kinome includes six more PKs that constitute such solitary branches stemming directly from the origin; four of these have already been characterized to some extent: p53-related protein kinase (*TP53RK*) (Abe et al., 2001), haspin (*GSG2*) (Tanaka et al., 1999) (all species, including yeast), *Slowpoke channel binding protein* (*Slob*) (Schopperle et al., 1998) (*Drosophila*) and phosphoinositide-3-kinase regulatory subunit 4 (*PIK3R4*; *VPS15*) (Herman et al., 1991). Homologs for all of these exist in both vertebrates and invertebrates. By contrast, to our knowledge there have been no previous reports regarding three other genes, including *Vlk*. Interestingly, our BLAST search of *SGK196* and *SGK396* similarly failed to find any homologs in invertebrates, as was the case for *Vlk*. The most homologous genes identified in this search outside of the vertebrate orthologs were from plant genomes for all three PKs. Thus, it is likely that these three PKs, including *Vlk*, might have newly evolved in vertebrates, although we cannot exclude the possibility that genome coverage in invertebrates is incomplete. Thus, all three PKs can be designated as vertebrate lonesome kinases. Further studies on the functions of the three Vlks might provide some insight into vertebrate evolution.

The *Vlk* gene product has at least seven subdomains characteristic of PKs, and it is likely that Vlk is a kinase. Subdomains V, IX, X and XI were not identified, but the presence of these domains varies among kinases. Subdomain VIII plays a major role in the recognition of peptide substrates and contains a well-conserved Ala-Pro-Glu (APE) triplet, but there is no APE sequence in kinase subdomain VIII of Vlk. This APE consensus is known to be required for the autophosphorylation activity of v-Src (Bryant and Parsons, 1984). This is consistent with our finding that Vlk does not have an autophosphorylation activity. Despite our failure to obtain direct biochemical evidence of the kinase activity of Vlk, we still surmise that Vlk is a PK for the following indirect reasons. Vlk transfected into HEK293T cells is phosphorylated at tyrosine 148 and serine 177. This tyrosine phosphorylation of Vlk requires the presence of the intact kinase domain of Vlk itself, as mutation of the ATP-binding site resulted in complete loss of phosphorylation. As the mutated Vlk is tyrosine phosphorylated when co-transfected with WT Vlk into the same cell, it would appear to be a substrate of a Vlk-dependent phosphorylation cascade. Moreover, in cells co-transfected with the two forms of Vlk, the WT and kinase-dead Vlk were co-immunoprecipitated. One parsimonious explanation for these observations is that Vlk forms a multimer in the cells, with members phosphorylating each other.

We showed that Vlk is enriched preferentially in the Golgi apparatus and that Vlk overexpression inhibits VSVG transport. This phenotype is dependent on the Golgi localization of Vlk but not on its phosphorylating activity. Hence, Vlk can be classified as a member of the Golgi membrane proteins that play a role in protein transport from Golgi to PM. However, the functional significance of the kinase activity of Vlk in the Golgi remains for future study. Various proteins, including caseins (Duncan et al., 2000; Turner et al., 1993; West and Clegg, 1984), proteoglycan (Glossl et al., 1986) and osteopontin (Lasa et al., 1997), are known to be phosphorylated in the Golgi. Hence, it is possible that Vlk is involved in the phosphorylation of such proteins in the Golgi.

It should be emphasized that *Vlk* expression is regulated by a developmental program and that mesenchymal cell lines, such as NIH3T3 or mouse embryonic fibroblast, do not express *Vlk*. During embryogenesis, the *Vlk* expression pattern is strictly regulated in a spatiotemporal manner, but the expression per se is widespread in all germ layers, such as in the AVE, ventral part of the midbrain and mesenchymal cells. *Vlk* appears to be specifically expressed in areas that are actively segregating from the surroundings, such as the Gsc^+ organizer, the AVE, condensed mesenchyme, hypertrophic chondrocytes and mesothelium. The phenotype of $Vlk^{-/-}$ mice indicates that many of these processes progress normally in such embryos. Even in areas where functional involvement of Vlk is evident, the defect is in most cases incomplete. For example, in $Vlk^{-/-}$ embryos endochondral ossification is delayed and the body size is small, but all processes required for chondrogenesis and subsequent osteogenesis are completed. Similarly, the elevation of the palatal shelf failed in most cases, although some proportion of palatal shelves underwent normal elevation. Finally, although the $Vlk^{-/-}$ mice died owing to respiratory failure, most offspring survived for up to a few hours, suggesting the presence of partially functioning lung structures. These results suggest that *Vlk* has a definite functional role in some, but not all, developmental processes with which its expression is associated, but its role in each process is as a modulator rather than as a master regulator or essential component. In all processes analyzed in the present study, lack of *Vlk* had no effect on cell proliferation or apoptosis of normally Vlk^+ cells. By contrast, the effect of the *Vlk*-null mutation was found in cells that do not normally express Vlk. In lung morphogenesis, the cells affected are Vlk^- alveolar cells, and in palate elevation Vlk appears to be involved in generating morphogenetic force. In both tissues, cells that are normally Vlk^+ are generated normally in the absence of *Vlk*. Thus, it is likely that Vlk is required for the functional activity of Vlk^+ cells to support the development of cells in their vicinity. By contrast, in endochondral ossification, defects were detected in the Vlk^+ cells themselves. Hence, Vlk can also be involved in the regulation of cell differentiation, or, alternatively, the delay of differentiation can be ascribed to defects in the surrounding environment to which differentiating chondrocytes themselves are likely to contribute.

Our cell biological analysis showing that expression of *Vlk* in the normally Vlk^- NIH3T3 cells suppresses VSVG-GFP transport is also consistent with the notion that Vlk is required for the formation of a proper environment for organogenesis. Of particular interest in this context is the striking similarity of $Vlk^{-/-}$ mice to those null for *Fgf18* or aggrecan, which encode proteins that are secreted into the extracellular space. $Fgf18^{-/-}$ mice die shortly after birth owing to a failure of alveolar development and show a delay in bone formation and a cleft palate (Liu et al., 2002; Ohbayashi et al., 2002). Interestingly, the cleft palate in this strain has been suggested to involve the failure of palate elevation. Cartilage matrix deficiency (*cmd*), a mouse strain with a spontaneous null mutation of the aggrecan gene, shows defects in bone formation, a cleft palate and respiratory failure (Watanabe et al., 1994). Obviously, there are some differences among these strains, but these defects common to all three mutant mouse strains strongly suggest that the formation of a proper environment expressing Fgf18 and aggrecan is essential for these developmental processes. Our present results thus suggest that Vlk is also involved in the formation of a functional extracellular matrix. Given that Vlk non-specifically retards protein transport from the Golgi, we would speculate that Vlk-mediated retention of proteins plays roles in the proper processing and assembly of proteins in the Golgi, thereby quantitatively increasing the amount of functional matrix proteins.

We thank the Laboratory for Animal Resources and Genetic Engineering for the generation of mutant mice and for the housing of mice; Drs T. Shimizu and M. Hibi for providing zebrafish materials; Drs M. Ikeya and Y. Sasai for providing materials for gene targeting; and Ms K. Shinmyozu for mass spectrometry analysis. This work was supported by grants from the Leading

Project for Realization of Regenerative Medicine (to S.N.), the Knowledge Cluster Initiative (to T.E.), the Ministry of Education and Science (grants 17045039 and 18052023) (to T.E.) and a grant-in-aid for scientific research from the Japan Society for the Promotion of Science (to M.K.).

Supplementary material

Supplementary material for this article is available at http://dev.biologists.org/cgi/content/full/136/12/2069/DC1

References

Abe, Y., Matsumoto, S., Wei, S., Nezu, K., Miyoshi, A., Kito, K., Ueda, N., Shigemoto, K., Hitsumoto, Y., Nikawa, J. et al. (2001). Cloning and characterization of a p53-related protein kinase expressed in interleukin-2-activated cytotoxic T-cells, epithelial tumor cell lines, and the testes. *J. Biol. Chem.* **276**, 44003-44011.

Bryant, D. L. and Parsons, J. T. (1984). Amino acid alterations within a highly conserved region of the Rous sarcoma virus src gene product pp60src inactivate tyrosine protein kinase activity. *Mol. Cell. Biol.* **4**, 862-866.

Caenepeel, S., Charydczak, G., Sudarsanam, S., Hunter, T. and Manning, G. (2004). The mouse kinome: discovery and comparative genomics of all mouse protein kinases. *Proc. Natl. Acad. Sci. USA* **101**, 11707-11712.

Duncan, J. S., Wilkinson, M. C. and Burgoyne, R. D. (2000). Purification of Golgi casein kinase from bovine milk. *Biochem. J.* **350**, 463-468.

Glossl, J., Hoppe, W. and Kresse, H. (1986). Post-translational phosphorylation of proteodermatan sulfate. *J. Biol. Chem.* **261**, 1920-1923.

Hanks, S. K. and Hunter, T. (1995). Protein kinases 6. The eukaryotic protein kinase superfamily: kinase (catalytic) domain structure and classification. *FASEB J.* **9**, 576-596.

Hanks, S. K., Quinn, A. M. and Hunter, T. (1988). The protein kinase family: conserved features and deduced phylogeny of the catalytic domains. *Science* **241**, 42-52.

Herman, P. K., Stack, J. H., DeModena, J. A. and Emr, S. D. (1991). A novel protein kinase homolog essential for protein sorting to the yeast lysosome-like vacuole. *Cell* **64**, 425-437.

Hirashima, M., Bernstein, A., Stanford, W. L. and Rossant, J. (2004). Gene-trap expression screening to identify endothelial-specific genes. *Blood* **104**, 711-718.

Hirschberg, K., Miller, C. M., Ellenberg, J., Presley, J. F., Siggia, E. D., Phair, R. D. and Lippincott-Schwartz, J. (1998). Kinetic analysis of secretory protein traffic and characterization of golgi to plasma membrane transport intermediates in living cells. *J. Cell Biol.* **143**, 1485-1503.

Ikeya, M., Kawada, M., Nakazawa, Y., Sakuragi, M., Sasai, N., Ueno, M., Kiyonari, H., Nakao, K. and Sasai, Y. (2005). Gene disruption/knock-in analysis of mONT3: vector construction by employing both in vivo and in vitro recombinations. *Int. J. Dev. Biol.* **49**, 807-823.

Karasawa, S., Araki, T., Nagai, T., Mizuno, H. and Miyawaki, A. (2004). Cyan-emitting and orange-emitting fluorescent proteins as a donor/acceptor pair for fluorescence resonance energy transfer. *Biochem. J.* **381**, 307-312.

Keller, G., Kennedy, M., Papayannopoulou, T. and Wiles, M. V. (1993). Hematopoietic commitment during embryonic stem cell differentiation in culture. *Mol. Cell. Biol.* **13**, 473-486.

Kimmel, C. A. and Trammell, C. (1981). A rapid procedure for routine double staining of cartilage and bone in fetal and adult animals. *Stain Technol.* **56**, 271-273.

Lasa, M., Marin, O. and Pinna, L. A. (1997). Rat liver Golgi apparatus contains a protein kinase similar to the casein kinase of lactating mammary gland. *Eur. J. Biochem.* **243**, 719-725.

Liu, Z., Xu, J., Colvin, J. S. and Ornitz, D. M. (2002). Coordination of chondrogenesis and osteogenesis by fibroblast growth factor 18. *Genes Dev.* **16**, 859-869.

Manning, G., Whyte, D. B., Martinez, R., Hunter, T. and Sudarsanam, S. (2002). The protein kinase complement of the human genome. *Science* **298**, 1912-1934.

Massaro, G. D. and Massaro, D. (1996). Formation of pulmonary alveoli and gas-exchange surface area: quantitation and regulation. *Annu. Rev. Physiol.* **58**, 73-92.

Nagai, T., Ibata, K., Park, E. S., Kubota, M., Mikoshiba, K. and Miyawaki, A. (2002). A variant of yellow fluorescent protein with fast and efficient maturation for cell-biological applications. *Nat. Biotechnol.* **20**, 87-90.

Ninomiya-Tsuji, J., Kishimoto, K., Hiyama, A., Inoue, J., Cao, Z. and Matsumoto, K. (1999). The kinase TAK1 can activate the NIK-I kappaB as well as the MAP kinase cascade in the IL-1 signalling pathway. *Nature* **398**, 252-256.

Nishikawa, S. I., Nishikawa, S., Hirashima, M., Matsuyoshi, N. and Kodama, H. (1998). Progressive lineage analysis by cell sorting and culture identifies FLK1+VE-cadherin+ cells at a diverging point of endothelial and hemopoietic lineages. *Development* **125**, 1747-1757.

Ohbayashi, N., Shibayama, M., Kurotaki, Y., Imanishi, M., Fujimori, T., Itoh, N. and Takada, S. (2002). FGF18 is required for normal cell proliferation and differentiation during osteogenesis and chondrogenesis. *Genes Dev.* **16**, 870-879.

Schopperle, W. M., Holmqvist, M. H., Zhou, Y., Wang, J., Wang, Z., Griffith, L. C., Keselman, I., Kusinitz, F., Dagan, D. and Levitan, I. B. (1998). Slob, a novel protein that interacts with the Slowpoke calcium-dependent potassium channel. *Neuron* **20**, 565-573.

Su, W. B., Chang, Y. H., Lin, W. W. and Hsieh, S. L. (2006). Differential regulation of interleukin-8 gene transcription by death receptor 3 (DR3) and type I TNF receptor (TNFRI). *Exp. Cell Res.* **312**, 266-277.

Tada, S., Era, T., Furusawa, C., Sakurai, H., Nishikawa, S., Kinoshita, M., Nakao, K., Chiba, T. and Nishikawa, S. (2005). Characterization of mesendoderm: a diverging point of the definitive endoderm and mesoderm in embryonic stem cell differentiation culture. *Development* **132**, 4363-4374.

Takebe, A., Era, T., Okada, M., Martin Jakt, L., Kuroda, Y. and Nishikawa, S. (2006). Microarray analysis of PDGFR alpha+ populations in ES cell differentiation culture identifies genes involved in differentiation of mesoderm and mesenchyme including ARID3b that is essential for development of embryonic mesenchymal cells. *Dev. Biol.* **293**, 25-37.

Tamura, K., Dudley, J., Nei, M. and Kumar, S. (2007). MEGA4: Molecular Evolutionary Genetics Analysis (MEGA) software version 4.0. *Mol. Biol. Evol.* **24**, 1596-1599.

Tanaka, H., Yoshimura, Y., Nozaki, M., Yomogida, K., Tsuchida, J., Tosaka, Y., Habu, T., Nakanishi, T., Okada, M., Nojima, H. et al. (1999). Identification and characterization of a haploid germ cell-specific nuclear protein kinase (Haspin) in spermatid nuclei and its effects on somatic cells. *J. Biol. Chem.* **274**, 17049-17057.

Thompson, J. D., Gibson, T. J., Plewniak, F., Jeanmougin, F. and Higgins, D. G. (1997). The CLUSTAL_X windows interface: flexible strategies for multiple sequence alignment aided by quality analysis tools. *Nucleic Acids Res.* **25**, 4876-4882.

Turner, M. D., Handel, S. E., Wilde, C. J. and Burgoyne, R. D. (1993). Differential effect of brefeldin A on phosphorylation of the caseins in lactating mouse mammary epithelial cells. *J. Cell Sci.* **106**, 1221-1226.

Watanabe, H., Kimata, K., Line, S., Strong, D., Gao, L. Y., Kozak, C. A. and Yamada, Y. (1994). Mouse cartilage matrix deficiency (cmd) caused by a 7 bp deletion in the aggrecan gene. *Nat. Genet.* **7**, 154-157.

West, D. W. and Clegg, R. A. (1984). Casein kinase activity in rat mammary gland Golgi vesicles. Demonstration of latency and requirement for a transmembrane ATP carrier. *Biochem. J.* **219**, 181-187.

Yagi, T., Tokunaga, T., Furuta, Y., Nada, S., Yoshida, M., Tsukada, T., Saga, Y., Takeda, N., Ikawa, Y. and Aizawa, S. (1993). A novel ES cell line, TT2, with high germline-differentiating potency. *Anal. Biochem.* **214**, 70-76.

Yasunaga, M., Tada, S., Torikai-Nishikawa, S., Nakano, Y., Okada, M., Jakt, L. M., Nishikawa, S., Chiba, T., Era, T. and Nishikawa, S. (2005). Induction and monitoring of definitive and visceral endoderm differentiation of mouse ES cells. *Nat. Biotechnol.* **23**, 1542-1550.